

Punctuated chaos and the unpredictability of the Galactic center S-star orbital evolution

Simon F. Portegies Zwart^{1*} and Tjarda C.N. Boekholt² and Douglas C. Heggie³

¹*Leiden Observatory, Leiden University, PO Box 9513, 2300 RA, Leiden, The Netherlands.*

²*Rudolf Peierls Centre for Theoretical Physics, Clarendon Laboratory, Parks Road, OX1 3PU, Oxford, UK.*

³*School of Mathematics and Maxwell Institute for Mathematical Sciences, University of Edinburgh, Kings Buildings, Edinburgh EH9 3FD, UK*

30 August 2023

ABSTRACT

We investigate the chaotic behavior of the S-star cluster in the Galactic center using precise N -body calculations, free from round-off or discretization errors. Our findings reveal that chaos among the Galactic center S-stars arises from close encounters, particularly among pairs and near the massive central body. These encounters induce perturbations, causing sudden changes in the orbital energies of the interacting stars. Consequently, neighboring solutions experience roughly exponential growth in separation. We propose a theory of "punctuated chaos" that describes the S-star cluster's chaotic behavior. This phenomenon results from nearly linear growth in the separation between neighboring orbits after repeated finite perturbations. Each participating star's orbit experiences discrete, abrupt changes in energy due to the perturbations. The cumulative effect of these events is further amplified by the steady drift in orbital phase. In the Galactic center, perturbations originate from coincidental encounters occurring within a distance of $\lesssim 100$ au between at least two stars (in some cases, three stars). Our model satisfactorily explains the observed exponential growth in the 27 S-star cluster. We determine that the S-star system has a Lyapunov time scale of approximately 462 ± 74 years. For the coming millennium, chaos in the S-star cluster will be driven mainly by a few of the closest orbiting stars: S2, S5, S6, S8, S9, S14, S18, S31, S21, S24, S27, S29, and S38.

Key words: Chaos – N -body simulations – supermassive black hole – S-stars – Galactic center

1 INTRODUCTION

Newton's laws of motion lead to chaos. This chaotic behavior is often quantified by measuring the growth in time of the separation, δ , between two neighbouring solutions, i.e. by solving the equations of motion of the multi-body system twice, once with and once without a small change in the initial conditions. If the evolution of δ is roughly exponential, but δ is still small by the end of the calculations, we call the evolution chaotic.

Chaotic behavior can be quantified using the Lyapunov time scale, which (in a more rigorous treatment) is the reciprocal of the maximum positive Lyapunov exponent. The Lyapunov time scale has been measured for only a limited number of multi-body systems, because these measurements are expensive in terms of computer time. It is not even clear that a specific system, within the uncertainty of its initial conditions, leads to a unique Lyapunov timescale, because the available parameter space may have an irregular structure with stable and chaotic regions (Hayes 2008).

In the Solar System, chaos is mainly driven by resonant overlap (Chirikov 1979; Wisdom 1980; Tamayo et al. 2021; Rath et al. 2022; Mogavero & Laskar 2022), which has some resemblance with resonant relaxation in the galactic center (Sridhar & Touma 2016), or even with violent relaxation (Kandrup et al. 2003). Previous studies, however, found that repeated weak scatterings among minor bod-

ies also form a major driver for changes in the orbital parameters, for example in studies on the orbit of mercury (Laskar & Gastineau 2009), but also in Halley's comet (Boekholt et al. 2016) to be chaotic on a time scale of less than 3000 years, as it interacts with Venus and Jupiter. In numerical studies of planet-planet scattering experiments in hypothetical multi-planet systems chaotic behavior is also recognized to be driven by encounters, rather than resonant overlap (Jurić & Tremaine 2008; Chatterjee et al. 2008). This event-driven chaotic behavior does not comply with Chirikov's resonant overlap paradigm.

This finding hints towards an event-driven process, where resonances are not required, but where chaos is driven by close encounters. We informally refer to such behaviour as "punctuated chaos". A similar chaotic behavior was found in stellar clusters (Goodman et al. 1993), where mutual interactions between stars seemed to drive chaos in the system. A system consisting of many eccentric and inclined orbits behaves differently from a flat system with non-crossing orbits and a dominant central body. The S-star cluster in the Galactic center (Ghez et al. 2008; Gillessen et al. 2009) may be a good example where resonant overlap does not form the major driver for chaos.

Understanding chaos in self-gravitating systems is important for understanding a wide variety of astronomical phenomena, including the sources of gravitational waves, extreme-mass-ratio inspirals, and the probability that a minor body hits the planet Earth. Our picture of punctuated chaos is also important for other Hamiltonian systems, such as the multi-body pendulum (Hoover & Griswold Hoover 2017),

* email: spz@strw.leidenuniv.nl

and it may be responsible for a slow-down of chaotic behavior in critical fluctuations (Das & Green 2019).

In our analysis of the S-stars, we will neglect low-mass stars, unobserved compact objects, and other interstellar material (planets, asteroids, dust, gas). The low-mass components are expected to be copious and important, but we limit ourselves to study chaos in an idealized system of black hole with S-stars. Chaos in the here studied idealised system then probably only provides an upper limit to the actual Lyapunov time scale.

2 CHAOS AS AN EVENT-DRIVEN PROCESS

2.1 The Lyapunov timescale

Consider a Keplerian two-body system, e.g. a star with a planet or supermassive black hole with a star. The difference between two neighbouring solutions, started with slightly different initial conditions, grows approximately linearly with time. The orbital phases of the two solutions gradually diverge, until their separation δ has grown to the size of the orbits.

In a three-body system consisting of a binary and a third body, the binary orbits are repeatedly perturbed by the third body. The effect of these events on two neighbouring binary orbits depends on their separation δ , and can cause the two solutions to diverge more quickly than in a two-body system. A sequence of perturbations, each with a subsequent period of linear divergence until the next perturbation, can then drive exponential divergence between two initially almost identical systems (Sec.2.2). The degree of chaos, measured in terms of the Lyapunov time scale, can then be derived by the frequency and strength of perturbations in the system (Sec.4.1).

In direct N -body calculations we can quantify chaos by measuring the Lyapunov time scale. Instead of a measure over the system's entire lifetime, which would be the setting for a rigorous treatment, a measure over a finite time interval is more practical in our case. We therefore define the growth factor $G_\delta(t)$ following from an initial separation $\delta(0)$ after some time t . The evolution of the separation is then described as an exponential function of time $\delta(t) = \delta(0)e^{\lambda t}$, where λ is the Lyapunov exponent. The growth factor can then be written as $G_\delta \equiv \delta(t)/\delta(0) = e^{\lambda t}$, and $\lambda = \log(G_\delta)/t$, or in terms of the Lyapunov timescale, $t_\lambda = 1/\lambda = t/\log(G_\delta)$.

2.2 Punctuated chaos

Based on the event-driven process described above, we derive approximate expressions for the Lyapunov time scale. We start again by considering a particle in a Kepler orbit around a much more massive body. With an initial semi-major axis a_0 , and total mass m the initial orbital frequency $\omega_0 = \sqrt{Gm/a_0^3}$. Let a neighboring solution be separated by an infinitesimal displacement δx_0 at time $t = 0$. This displacement leads to a small difference in the semi-major axis of the same order, i.e. $\delta a_0 \sim \delta x_0$. The resulting difference in frequency is

$$\delta\omega_0 \sim \delta x_0 \sqrt{Gm/a_0^5}. \quad (1)$$

The separation of the two motions along the orbit grows with time $t > 0$ according to

$$\delta x(t) \sim \delta x_0 + \delta\omega_0 a_0 t = \delta x_0 (1 + \omega_0 t). \quad (2)$$

The growth of the initial displacement is linear with time from t_0 to t , but such that δa remains constant as the growth is along the orbit, i.e. the growth is in orbital phase rather than in energy (or angular momentum).

Now suppose that an instantaneous perturbation acts on the motion at time t_1 , causing the velocity of the Kepler motion to receive a slight kick.

There is a resulting change in energy, and therefore a change in semi-major axis Δa_1 . But since the perturbation will depend on the position of the body, the *difference* in semi-major axis between the two motions, δa , will also change, by an amount which we call δa_1 . We suppose for the sake of argument that $\delta a_1 \sim \delta x_1$, i.e. the difference in position at the time of the event. (In Sec.4.1 we give a specific example in which it is easy to see that $\delta a_1 \propto \delta x_1$.) The new difference in semi-major axis implies a difference in orbital frequency $\delta\omega_1 \sim \delta a_1 \omega_1 / a_1$ at time t_1 . Thus for $t > t_1$ the displacement varies as

$$\begin{aligned} \delta x &\sim \delta x_1 + \omega_1 (t - t_1) \delta a_1 \\ &\sim \delta x_1 (1 + \omega_1 (t - t_1)). \end{aligned} \quad (3)$$

If a second perturbation occurs at time $t_2 > t_1$, we can see from eqs.2 and 3 that the displacement is

$$\delta x_2 \sim \delta x_0 (1 + \omega_0 t_1) (1 + \omega_1 (t_2 - t_1)). \quad (4)$$

If these perturbations recur at roughly comparable intervals Δt , and if ω does not change by a large factor, it can be seen that the displacement at some large time t will be

$$\delta x(t) \sim \delta x_0 (1 + \omega \Delta t)^{t/\Delta t}. \quad (5)$$

Thus the linear growth of eq. 2 transforms into exponential growth. The corresponding Lyapunov exponent is $O(\omega)$ if $\omega \Delta t \lesssim 1$; it is of order the reciprocal of the crossing time. The case $\omega \Delta t \gtrsim 1$ is also of interest and leads to a smaller estimate of order $\ln(\omega \Delta t)/\Delta t$.

Though we here considered perturbed Keplerian motion with one dominant body, which is relevant to our discussion of the S-stars in Sections 3 and 4, the conclusions are valid more widely. As an example, we consider resonant three-body scattering events, which can be viewed as a prolonged sequence of perturbations of the Kepler motion. So long as the three particles remain democratic (i.e., at comparable distances) and are of comparable mass, the perturbations in any of the three two-body motions will be of order unity and occur at intervals of order the crossing time, t_{cr} . Therefore, as in the above discussion, the Lyapunov exponent will be of order $1/t_{cr}$. Numerical examples of Dejonghe & Hut (1986) indeed show that the separation of neighboring solutions grows roughly exponentially until dissolution of the resonance (in the sense of a democratic three-body behaviour). On the other hand, if the evolution of a triple system is dominated by protracted excursions of the third body, of order $T \gg t_{cr}$, then the estimate will decrease to one of order $1/T$ (following the result for the case $\omega \Delta t \gtrsim 1$, and neglecting a logarithm). Usually, the evolution is a mix of prolonged excursions interspersed with periods of frequent interplay (Szebehely 1971), and the Lyapunov exponent λ will be $1/T \lesssim \lambda < 1/t_{cr}$, where T is the duration of the longest excursion. The lifetime of the Pythagorean problem, for example, is about $16t_{cr}$ (Aarseth 2003, their p.238), and the growth of the separation of neighboring solutions in this time is about 8.5 dex (Dejonghe & Hut 1986). Thus $T \lesssim 16t_{cr}$ and $\lambda \simeq 1.2/t_{cr}$, and the finite-time Lyapunov exponent lies in the range $1/T \lesssim \lambda \lesssim 1/t_{cr}$.

The result of the model (that the Lyapunov exponent λ is of order $1/t_{cr}$ for comparable masses without lengthy excursions) is consistent with the results in Goodman et al. (1993), who considered the general N -body problem. This is a rather independent confirmation, as their model was also based on assuming that the separation between neighboring solutions grows as a result of two-body encounters (see Tab. 1, but otherwise did not follow the same approach as ours).

3 APPLICATION OF PUNCTUATED CHAOS

We now study punctuated chaos in an actual astrophysical system, namely the S-star cluster in the Galactic center. All stars affect each other and we therefore stretch the assumptions of extreme mass ratio, the approximation of only two orbiting particles, and the three-dimensional nature of the problem.

Our analysis starts by acquiring converged solutions for the dynamical evolution of the S-stars. Acquiring a converged solution is important because round-off and discretization errors grow exponentially, rendering a non-converged solution inappropriate for studying chaos. We acquire converged solutions to the N -body problem by integrating Newton's equations of motion. The dynamics near supermassive black holes is best described with general relativity rather than by Newtonian dynamics. Still we perform our simulations using a Newtonian approximation and ignore the theory of general relativity. We consider this appropriate because the highest speed in our simulations (the star S2 at pericenter) does not exceed about ~ 0.017 times the speed of light. At these relatively low speeds, the system behaves like a Newtonian system, at least within our brief simulation time of 10^4 years (Portegies Zwart et al. 2022). In addition, our model for punctuated chaos was derived for Newtonian systems. In the presence of the black hole, in future it will be worth exploring the effect of general relativity on the chaotic behavior of the S-star cluster.

The results presented here are acquired using converged solutions. These result from a procedure in which the length of the mantissa, controlling precision, and the accuracy of the integrator are improved at each iteration step, as is explained in Portegies Zwart & Boekholt (2018). Such converged solutions can be achieved using Brutus. In Brutus, we control round-off by extending the numerical precision, and accuracy by reducing the tolerance in the Bulirsch-Stoer integrator (Bulirsch & Stoer 1964). By repeating the same calculation with higher precision and better accuracy, we eventually reach a solution for which the results remain identical to a pre-determined number of decimal places; we call this the converged solution.

3.1 Measuring chaos in the S-star cluster

We consider a realization of the S-star cluster, consisting of 27 early-type stars that orbit the supermassive black hole in the Galactic center. We adopted the orbital parameters of the 27 S-stars reported in Gillessen et al. (2009) (their table 7). The numbering of these stars is not simply S1 to S27, because we only use those stars for which an orbit is determined.

The initial conditions are generated using the AMUSE (Portegies Zwart et al. 2013; Pelupessy et al. 2013) routine `generate_Sstar_cluster.py` from Portegies Zwart & McMillan (2018). This routine adopts the cited orbital elements for the S-stars, and solves Kepler's equation to acquire Cartesian coordinates and velocities of the S-stars. We assume each S-star to have a mass of $20 M_{\odot}$, and adopt the central massive black hole mass of $4.154 \cdot 10^6 M_{\odot}$ (Gravity Collaboration et al. 2019). We integrate this system for 10000 yr until the solution converges using Brutus (Boekholt & Portegies Zwart 2015).

In figure 1 we present the converged solution of the projected orbits of the S-stars integrated over 10000 years. This solution was obtained using a word-length $L_w = 128$ bits, and a tolerance in the Bulirsch-Stoer integrator of $\epsilon = 10^{-24}$ leading to a total final phase-space error less than $1/10^7$, and a relative energy error in the integration of $dE/E \approx 10^{-15}$. Each calculation took about 20 hours on the single core of a Xeon W-11855M-processor. For $L_w = 116$ bit

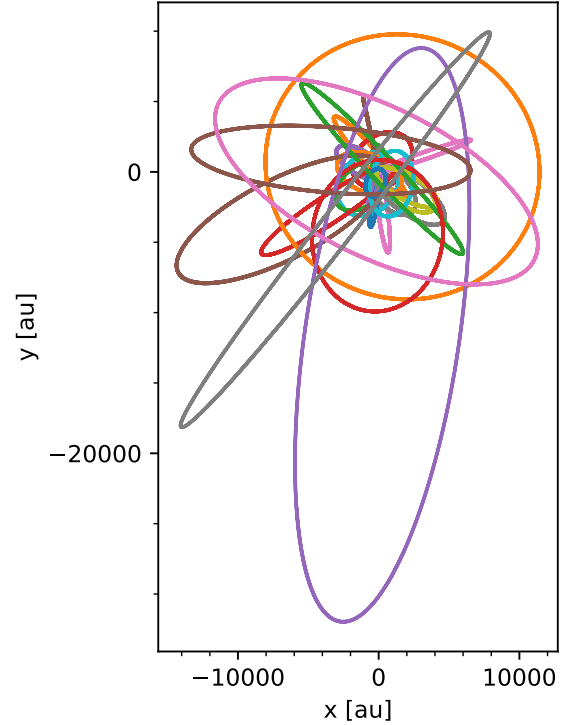


Figure 1. Projection of the S-stars' orbits in the y - x plane. These orbits are integrated for 10000 years from January 1st 2001 to 12001 yr. Even the widest orbits (star S83 has an orbital period of ~ 1700 yr) are overplotted several times. The orbits look Keplerian, but when we zoom in on any orbital segment, the fine structure of the chaotic orbital evolution becomes visible (see figure 2).

precision and a tolerance of $\epsilon = 10^{-21}$ the solution is converged to 4 decimal places, which would have sufficed for this study. Regular double precision, however, would have been insufficiently precise and would not have led to the required accuracy.

Although the orbits in figure 1 appear to follow a Keplerian orbit nicely, in figure 2 we show that this is not the case. Here we show a detail of the orbits of several stars from figure 1. Each orbital revolution is indicated with a thin line. The lines do not fully overlap, indicating that their orbits change with time.

After having established a converged simulation for the S-stars (see figure 1), we introduce a relative shift by translating the Cartesian x coordinate of Star S5 by 10^{-10} . This amounts to moving the initial position of S5 by ~ 15 m in the x direction.

Instead of the separation in position space for each individual S-star, as illustrated in figure 1, we can also present the more usual total phase-space distance as a function of time, which we define as (Dejonghe & Hut 1986)

$$\ln(\delta) = \frac{1}{2} \ln \left(\sum_{i=0}^n |\vec{r}_{i,1} - \vec{r}_{i,0}|^2 + |\vec{v}_{i,1} - \vec{v}_{i,0}|^2 \right). \quad (6)$$

Here 0 and 1 refer to the original and shifted solution, respectively. In figure 3 we present the evolution of the phase-space distance between the two solutions. The overplotted dotted line (in red) corresponds to a Lyapunov time scale of $t_{\lambda} \approx 450$ yr.

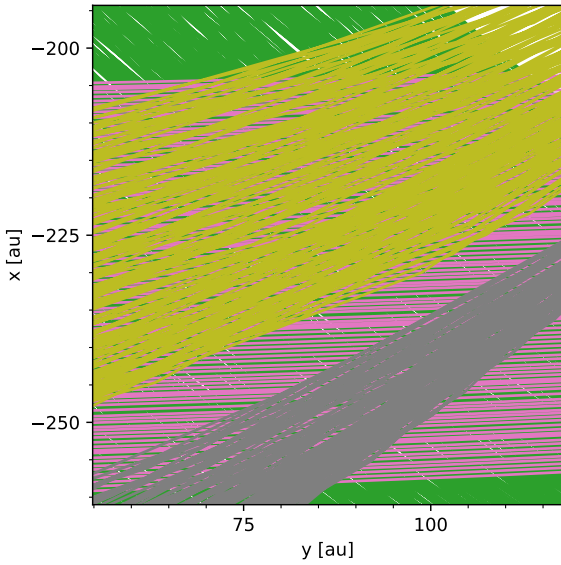


Figure 2. Magnification of a small section of the orbit of four S-stars over 10 000 yr of evolution. The orbit-to-orbit variation is small, and not noticeable in figure 1, but in this magnification the effect of chaos is visible in the non-overlapping orbits.

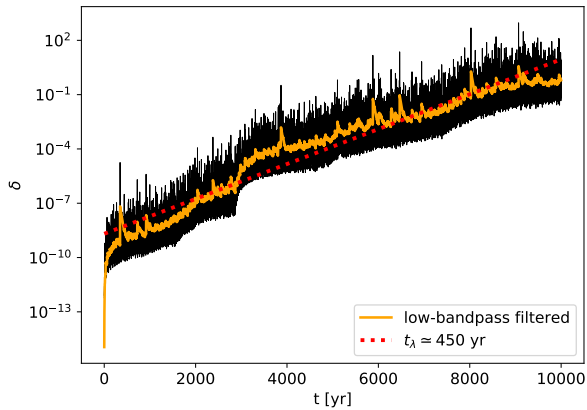


Figure 3. Evolution of the phase-space distance (eq.6) for the S-stars as a function of time (black). Here we adopted the phase-space difference between two solutions (the canonical initial conditions and the initial conditions with a displacement of star S5 by 10^{-10} in x); both are calculated using $\epsilon = 10^{-24}$ ($Lw = 128$ bits). Overplotted (in orange) is a filtered version of the data using a Butterworth (1930) low-bandpass filter of order 1. The dotted line gives a least-squares fit to the simulation data and indicates a Lyapunov time scale of $t_\lambda \approx 450$ year (red, as indicated).

In figure 4 we present the evolution of the root-mean-square difference in the semi-major axes between the two solutions for the S-stars. Here we define

$$\delta_a^2 = \frac{1}{n} \sum_{i=0}^n |a_{i,0} - a_{i,1}|^2. \quad (7)$$

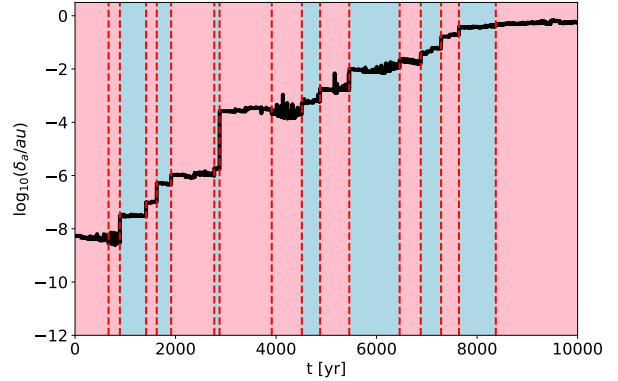


Figure 4. Growth of the root mean square difference in the semi-major axes, δ_a (eq.7), between the two solutions. The events are identified with the vertical red dashes. The color changes are introduced when the events lead to a growth in δ_a . Two negative events are also identified, one around 667 yr and at 3914 yr. The largest event occurs around 2876 years.

The events are visible at discrete times followed by a constant difference δ_a . In figure 3 a particularly strong event is visible in the phase-space distance evolution around $t = 2876$ years. According to punctuated chaos the orbital separation changes abruptly during events. We identify several with the colors and the vertical dashed lines (see figure 4). We automatically recognize these events in the simulation data using the Pelt algorithm (Killick et al. 2012), using the piecewise constant model. Both free parameters in the Pelt algorithm (the controls the minimum distance between change points and the grid of possible change points) were set to unity.

To further investigate which stars are involved, we apply the Pelt algorithm to individual stars. Three examples are presented in figure 5. Here the colors are meant to guide the eye and indicate the events already identified on the full set of 27 stars in figure 4. The vertical red-dashed lines are the events as identified using the Pelt algorithm for each individual star.

In table 1 we present the times at which events were detected, which stars are associated with these events, and at what distance from the black hole (in terms of au and in distance with respect to the sum of the stars' Hill radii). The stars S2 and S18, are frequent participants, and they form the main drivers of chaos. We also present in table 1 the values for r_{ij} , and r_{ij}/r_H . The former is defined as the distance between the two stars i and j nearest to the black hole at the moment of closest approach to the black hole. The latter gives the relative distance in terms of the radius of the Hill sphere of the two participating stars (second column). The last column gives the relative velocity between the two S-stars at the moment of closest mutual approach.

In figure 6, we present the results of applying the theory of punctuated chaos to the evolution of the S-star cluster over 10 000 years. Here we overplotted the actual data and the filtered curve, as in figure 3. The red curve results from measuring the time and magnitude of the events in semi-major axis (see figure 4 and table 1), which are then applied directly to our model for punctuated chaos (see section 2.2).

In the appendix we present the algorithm, based on equation 6 that is used to draw the red curve in figure 6. The events (moments of close encounter and the mutual distance between the two S-stars at peribothron) are measured in the N-body simulations, and presented

Table 1. Moments of close encounters between two of the S stars (T , second column) and the black hole. The third column gives the distance (D , rounded to au) from the closest of the two stars to the black hole. The subsequent column gives the mutual distance between the two S-stars (r_{ij}), followed by the mutual distance (r_{ij}) as fraction of the sum of the S-star’s Hill radii. The last column gives the relative velocity (rounded to 10km/s) between the two encountering stars (in km/s). Each of these events can also be identified in the growth of the semi-major axis of the two identified stars (see also figure 4). This data can be used directly in the small routine to calculate the phase-space distance evolution of the S-stars using our presented theory on Punctuated Chaos (see appendix). Note that in the big event at $T = 2876$ yr, also stars S9 and S14 participate (see figure 7).

T [yr]	participating stars	D [au]	r_{ij} [au]	r_{ij}/r_H	V_{ij} [km/s]
12.5	S38,S24	842	48.7	5.2	5060
407.8	S24,S38	952	43.3	4.6	4650
807.3	S29,S21	373	49.5	6.5	6030
1571.8	S38,S2	287	32.6	8.1	5580
1649.7	S2,S18	516	42.2	6.7	3350
1665.7	S2,S38	282	38.0	7.0	5580
2023.8	S5,S14	780	55.8	11.9	4800
2745.9	S2,S31	448	52.1	15.8	6170
2875.7	S6,S21	635	13.5	1.5	3900
3972.0	S5,S9	488	56.5	6.5	3660
4875.7	S8,S27	720	54.0	6.0	3520
6878.3	S2,S18	512	30.4	4.0	3210
7007.0	S2,S18	479	50.5	6.7	5420

in table 1. Note that several punctuated events listed in table 1 are not directly related to the jumps in semi-major axis presented in figure 4 (see also equation 7). For individual stars these jumps are visible, but they tend to be obscured by the ensemble averaging. Each of the events listed in table 1, however, do relate to a jump in semi-major axis in the S-stars associated with the close encounter. These jumps are visible in the evolution of the semi-major axis for individual S-stars; as examples we present this evolution for S6, S27 and S66 in figure 5, which also show the early (13 yr, 408 yr and 807 yr) and late (7007 yr) jumps listed in table 1 (red dashed lines).

The comparison between the theory and the simulations is striking. Although the red curve in figure 6 does not perfectly match the filtered curve (black), it is astonishingly similar. A slight deviation where the red curve overshoots the black curve, around $t = 7007$ yr, seem to be caused by several close encounters between S2 and S18. In our model, we anticipate on stand alone encounters, and the effect of multiple encounters in short succession between the same stars can also cause the evolution of δ to decay.

3.2 The big event at 2876 years

The largest event happens around $t = 2876$ yr after the start of the simulations.

In figure 7 we present the distance of the nearest star to the black hole (blue), and the distance between this star and its next nearest stellar neighbor (orange), around the moment of the big event at $t = 2876$ yr. Along the top we identify the stars involved in their close proximity. It starts at $t = 2870$ with S2 being the closest to the black hole, and S14 being closest to S2. At $t \approx 2872$ star S6 takes over the closest position to S2 from S14. At $t \approx 2873$ star S6 becomes the closest star to the black hole and at $t \approx 2874$ star S21 becomes the closest neighbor of star S6, until a little before $t = 2876$ star S6 and S21 have their mutual close encounter with each other and with the black hole.

In figure 8 we present for the stars S6 and S21 the evolution of

δ_r (left panels), i.e. the spatial separation between the two orbits; the semi-major axis (middle) and the difference in orbital frequency (right panels) around the moment of the big event at $t = 2876$ yr. In the evolution of the spatial separation (left) the consequences of the event are visible. The main driver of this evolution is the almost instantaneous change in orbital energy (middle panel, expressed here in semi-major axis) and the separation in orbital frequency (right-most panel).

4 DYNAMICS OF PUNCTUATED CHAOS IN THE S-STARS

The picture of punctuated chaos in Sec.2.2 lacks any dynamical characterisation of the events. They are simply circumstances which change the frequency of the orbital motion. Even at the close of Sect.3.1, in the construction of figure 6, the data on the changes in frequency is simply read from a full numerical simulation. In the present subsection we attempt to explain, in order of magnitude, how these changes arise, on the basis of few-body interactions.

For the purposes of this discussion, let us reduce the problem to a 3-body system consisting of a black hole (mass M , particle 0) and two S-stars (mass m , particles 1,2). Let \mathbf{r}_i be the position vector of star i relative to the black hole, and focus on star 1. Its equation of motion is

$$\ddot{\mathbf{r}}_1 = -\frac{G(M+m)\mathbf{r}_1}{r_1^3} - \frac{Gm(\mathbf{r}_1 - \mathbf{r}_2)}{r_{12}^3} - \frac{Gm\mathbf{r}_2}{r_2^3} \quad (8)$$

with obvious notation r_i, r_{12} . The first term on the right is the acceleration of the motion of star 1 relative to the black hole, the second term is the direct perturbation by particle 2, and the third term is the indirect perturbation, caused by the acceleration of the black hole by particle 2. (If we were to write down the equation for the case of N S-stars, the second and third terms on the right would be replaced by sums from $j = 2$ to N , with the index 2 replaced by j .)

4.1 Direct perturbations

From the previous section (especially figure 7 and table 1), we know empirically that the major events are associated with a close approach (to a distance of order 10–50 au) between two stars (see table 1), at times where the distances to the black hole are larger by an order of magnitude. If we label the stars in the encounter as 1 and 2 (ignoring all other stars for the time being), then it is clear that the perturbation on the motion of particle 1 is dominated by the second term on the right of eq.(8), i.e. the direct perturbation, due to the gravitational attraction of star 2. For the moment we also ignore the third term, but return to it briefly in Sec.4.2.

We now consider the growth of chaos in the single S-star which we have hitherto labelled as star 1, and suppose that it has a succession of close encounters with other stars (in “events”) at some interval Δt . Let δx denote the variation in some quantity x , such as energy or position, between two neighbouring solutions. Specifically, let δE_0 be the variation in specific energy $E \equiv |v|^2/2 - GM/r$ at a time just before an event, where v is the speed, and let δr_0 be the variation in position at the same time. (Henceforth the subscripts denote an index of events in a sequence of events.)

Then we have

$$\delta E_1 = \delta E_0 + \delta \Delta E, \quad (9)$$

where δE_1 is the variation just before the next event, which will be

the same as the value just after the first event; and ΔE is the change in E at that first event. Now we estimate this as

$$\Delta E = v\Delta v \sim \sqrt{GM/r} \frac{Gm}{Vd}, \quad (10)$$

where d is the distance of closest approach in the encounter, and V is the relative speed of the two stars in the encounter. Both these parameters are listed for the punctuations measured in the S-star cluster in table 1. (This estimate is made by taking Δv to be the maximum perturbation Gm/d^2 multiplied by the time scale of the encounter, d/V .) We use the same estimate $\sqrt{GM/r}$ for V as for v , so that

$$\Delta E \sim Gm/d, \quad (11)$$

Its variation can be estimated as

$$\delta(\Delta E) \sim \frac{Gm}{d^2} \delta r_0, \quad (12)$$

and so eq.(9) becomes

$$\delta E_1 \sim \delta E_0 + \frac{Gm}{d^2} \delta r_0. \quad (13)$$

After this event the variation in the orbital frequency will be $\delta\omega_1$, and so

$$\delta r_1 \sim \delta r_0 + \delta\omega_1 a \Delta t, \quad (14)$$

where a is the semi-major axis, just as in the simplified model of punctuated chaos described in Sec.2.2. Since $\omega^2 a^3 = GM$ and $E \sim GM/a$ (though strictly here, M should be replaced by $M+m$, but we ignore the stellar mass compared with the black hole mass.), we can reexpress this as

$$\delta r_1 \sim \delta r_0 + \delta E_1 \Delta t / \sqrt{GM/a}. \quad (15)$$

By eq.(13), this in turn becomes

$$\delta r_1 \sim \delta r_0 + (\delta E_0 + \frac{Gm}{d^2} \delta r_0) \Delta t / \sqrt{GM/a}. \quad (16)$$

Equations (13) and (16) are explicit estimates which allow us to map the effect of an encounter on δE and δr . It has matrix

$$A = \begin{pmatrix} 1 & Gm/d^2 \\ \Delta t / \sqrt{GM/a} & 1 + (Gm/d^2) \Delta t / \sqrt{GM/a} \end{pmatrix}.$$

The larger eigenvalue of this matrix gives the factor by which the variation, in either E or r , is multiplied as a result of an event.

To get a feel for the magnitude of this evolution, consider the six encounters in Table 1 which involve star S2. The mean distance of closest approach in these is about 40 au, which we take for the value of d . Since the duration of the simulation is 10 000 yr, for the mean time between these six events we adopt $\Delta t = 1700$ yr. The semi-major axis of S2 is $a_{S2} \approx 1000$ au, and we take $m = 20 M_\odot$ and $M = 4 \times 10^6 M_\odot$, as we have done throughout. (These units imply that $G = 4n^2 \sim 40$.) Then the quantity

$$Gm/d^2 \Delta t / \sqrt{GM/a} \sim 2, \quad (17)$$

and the larger eigenvalue $\lambda \approx 4$. Thus the variations increase by this factor in 1700 yr, or by almost 4 dex in 10^4 yr. While this estimate is only about half of the logarithmic growth seen in figures 3 and 6, it only includes half of the events listed in Table 1. The remaining events involve stars other than S2, which is why they were omitted from this estimate, but we show in Sec.4.2 how their influence spreads to all stars, S2 included.

The foregoing argument can be criticised on several grounds, and the main one is that it still depends on the numerical integration, as it

draws on the distance of the observed two-body encounters. This may be estimated independently as follows. From the initial conditions of the integration we can estimate the central number-density n of the S-star cluster from the distance of the 6th-nearest neighbour to the black hole (Hénon 1971), which is about 2000 au. Hence $n \approx 2 \times 10^{-10}$. The median semi-major axis a is about 3000 au, and so we may estimate the typical speed $v = \sqrt{GM/a}$ as about 200 au/yr. It follows that a typical S-star i will experience one two-body encounter with another S-star j in 10^4 yr at a distance less than about $r_{ij} \approx 60$ au. One or two will do so at still smaller distances, consistent with what is seen in the numerical results.

4.2 The role of the indirect acceleration

While Sec.4.1 makes a reasonable case for supposing that direct encounters between pairs of S-stars are a major driver of chaos in the system, it is not clear how many stars are affected, as only a fraction of all S-stars appear in Tables 1. Of course all stars are subject to two-body direct perturbations, but it might be thought that weak perturbations would drive chaos on a longer timescale. We now consider the effect of indirect perturbations, and will show that these affect all stars. Furthermore they keep the growth of chaos in all stars in lockstep.

The indirect perturbation of star 2 in eq.(8) is given by the third term on the right, and clearly depends on its distance r_2 from the black hole. Thus we shall consider the pericentre passages of star 2 as the driver of this component of punctuated chaos. In one such event, whose duration is of order q/v_2 , where q is the pericentre distance of star 2, the change in energy of star 1 may be estimated as

$$\Delta E \sim v_1 Gm / (qv_2). \quad (18)$$

Much as in Sec.4.1, we estimate $v_2 \sim \sqrt{GM/q}$, but for the first star we take $v_1 \sim \sqrt{GM/a}$, where a is the semi-major axis of star 1, since this star can be anywhere on its orbit when the event occurs. Thus

$$\Delta E \sim Gm / \sqrt{aq}, \quad (19)$$

and so the variation in this quantity is

$$\delta(\Delta E) \sim \delta q Gm / \sqrt{aq^3}. \quad (20)$$

Now suppose that star 2 is one of those which is vigorously affected by direct interactions with other stars, and its variations have Lyapunov exponent λ . Then we can estimate that

$$\delta q \sim \delta q_0 \exp(\lambda t), \quad (21)$$

where δq_0 is some constant. Next, substituting this estimate into eq.(20), and adding the effect of a succession of such events, we readily see that the sum of the corresponding exponentials can be estimated by the effect of the most recent event. Thus the variation in the energy of star 1 at time t may be estimated as

$$\delta E \sim \delta q_0 \exp(\lambda t) Gm / \sqrt{aq^3}. \quad (22)$$

Thus we conclude that chaos in star 1 grows with the same Lyapunov exponent as star 2, and this would be true even if star 1 were not subject to any direct perturbations.

In figure 9, we plot the time evolution of the separation in position space for each of the 27 S-stars, as well as for the central black hole. We observe that, on average, all particles diverge exponentially and with roughly the same rate. By fitting linear slopes to each curve in the figure, we measure an average individual Lyapunov time scale of 462 ± 74 years. Figure 9 shows that all stars, and also the central black hole, diverge at the same rate on average. For the black hole

the amplitude is smaller than for the bulk of the S-stars by roughly the ratio of their masses, i.e. 2×10^5 .

5 CONCLUSIONS

In order to explain short time-scale chaos in self-gravitating democratic dynamical systems, we outline the theory of punctuated chaos. The essence of punctuated chaos is that instantaneous close encounters, or events, drive the exponential growth due to ephemeral perturbations, each of which is followed by a gradual drift in phase space. Our description of punctuated chaos delivers a qualitative and quantitative description of chaos in self-gravitating systems.

We test this description on converged direct N -body simulations of self-gravitating systems under Newton's equations of motion. We confirm the working of punctuated chaos on the chaotic orbits of the S-stars in orbit around the supermassive black hole in the Galactic center. The rather similar values of the mean orbital period of the S-stars and their Lyapunov time scale then is no coincidence.

It turns out that also comet Halley has a Lyapunov time scale quite comparable to its orbital period (Boekholt et al. 2016). In this case the chaos is driven by interaction with Venus and Jupiter. We argue that the Lyapunov time scale under punctuated chaos is proportional to the mean interacting orbital period of the system, which for our selected systems is of the order of a few 100 years.

According to our arguments and findings (Section 4.2), major bodies are affected on a similar time scale, but the amplitude δ scales roughly with the ratio of the perturber to the perturbed mass, as one sees for the black hole in Fig. 9.

For the 27 S-stars in the Galactic center, we derive a Lyapunov time scale of 462 ± 74 yr. This is somewhat comparable to the mean orbital period of the S-stars, or $\langle P_{\text{orb}} \rangle = 269 \pm 383$ yr, consistent with the prediction from punctuated chaos.

We also qualitatively compare the measured phase-space distance evolution with the theory of punctuated chaos (see Section 3.1, especially Fig. 6).

In the theory (Sec. 3), the number of interactions (events) and the strength of these interactions are free parameters. In the comparison presented in Fig. 6, the moment and strength of each interaction are measured through an N -body simulation. But we also show (Sec. 4.1) that these parameters can be estimated in order of magnitude without resort to an N -body simulation, but from estimates of the density and kinematics of the inner S-stars. This procedure allows us to directly compare the theory with the simulations, as well as to identify the events that drive the exponential growth.

If the previous analysis holds, chaos manifests itself from repeated small perturbations that each induce a linear response in the separation between neighbouring solutions of the system. The composition of these linear responses resembles an exponential behavior and drives chaos in the system. The perturbation, initiated by a close encounter between two (or more) stars, is subsequently communicated to the rest of the system by the perturbed phase-space characteristics of the massive central body. In the case of the S-stars this is the super-massive black hole, and it is the Sun for comet Halley and the rest of the Solar system. In this way the entire system is subject to the same smallest Lyapunov time scale.

ACKNOWLEDGEMENTS

It is a pleasure to thank Geneva Observatory and in particular, George Meylan, Silvia Extröm, and Steven Rieder for their hospitality. This

work started with the Masters' thesis of Jaro Molemkamp at Leiden University under the co-supervision of Veronica Saz Ulibarrena.

The first author thanks Deutsche Bahn for the availability of green electricity in combination with long delays on trips to from Amsterdam to Geneva, Copenhagen, and München, which enabled part of the writing, further code development and verification calculations.

Computing resources

The majority of the computational resources were provided by the Academic Leiden Interdisciplinary Cluster Environment (ALICE), and using LGM-II (NWO grant # 621.016.701). Software we used include AMUSE (Portegies Zwart et al. 2018), Python (Van Rossum & Drake 2009), Pelt (Killick et al. 2012), Numpy (Oliphant 2006), Scipy (Jones et al. 01), MPFR (Fousse et al. 2007), Brutus (Boekholt & Portegies Zwart 2015), Matplotlib (Hunter 2007), Linux (see <https://github.com/torvalds/linux/releases/tag/v4.1-rc8>).

Energy consumption of this calculation

The calculations using Brutus are elaborate and took about $7 \cdot 10^6$ CPU seconds. Data processing and analysis require about one tenth, totalling about three months of dual CPU usage. Using the tool <http://green-algorithms.org/> and Portegies Zwart (2020), we calculated our energy consumption to be about 160 KWh.

DATA AVAILABILITY

Raw and reduced data, and processing scripts are available at figshare DOI: 10.6084/m9.figshare.13637672

APPENDIX: CALCULATING THE EVOLUTION OF THE PHASE-SPACE DISTANCE

We calculate the evolution of the phase space distance, as presented in figure 6 (red curve) using the algorithms presented in the form of a Python script using the units module from the Astrophysics Multipurpose software Environment (AMUSE Portegies Zwart & McMillan 2018) in the listing below. The events (time T and mutual distance r_{ij} between the two closest S-stars i and j near the black hole) used to draw the curves are presented in table 1. These events were automatically detected by identifying the closest encounters between at least two stars near the black hole. Here we included only those encounters with a mutual distance $r_{ij} \lesssim 60$ au. We introduce the constant $k = 0.5$ au which relates the effect of the perturbation to the orbital deviation. Looping over time, we calculate the new phase-space distance between the two solutions, given the perturbation introduced in the last close encounter (see equation 3). We empirially determine $\omega_1 \propto (k/r_{ij})^2$ from the N -body simulations by measuring r_{ij} and fitting k based on the evolution of the growth of the phase-space distance δ (see equation. 6). The stated dependence on r_{ij} here is justified by the d -dependence in equation 13.

```
from amuse.lab import units
def phase_space_distance(T, rij, k=4|units.au):
    delta = [0] | units.m
    t = [0] | units.yr
    dd = [1] | units.m
    while t[-1] < T[-1]:
        d = dd[-1]*(1+((t[-1]-T[ len(dd) -1]).
            value_in(units.yr))*(k/rij[ len(dd) -1])
            **2)
        if t[-1] >= T[ len(dd) ]:
            dd.append(d)
        t.append(t[-1]+dt)
        delta.append(d)
```

```
return t, delta
```

The input arrays, T and ri_j are determined from close encounters between the S-stars and the black hole, as explained in Section 3.1, and present in table 1. Note that these encounters are not all the same as those identified using the Pelt algorithm in figure 4 because some close encounters do not show up as prominently in the global evolution of the orbital separation (see equation 7), but they do appear in the individual evolution of the semi-major axis of the S-stars. For S6, S21 and S66 these data are presented in figure 5. In particular the earlier encounters at 13 yr and 408 yr, and the late encounter at 9046 yr do not appear from the analysis of the global change in semi-major axis through the Pelt algorithm, but they are visible as jumps in the evolution of the individual S-stars.

REFERENCES

- Aarseth S. A., 2003, Gravitational N-body simulations. Cambridge University press, 2003
- Boekholt T., Portegies Zwart S., 2015, *Computational Astrophysics and Cosmology*, 2, 2
- Boekholt T. C. N., Pelupessy F. I., Heggie D. C., Portegies Zwart S. F., 2016, *MNRAS*, 461, 3576
- Bulirsch R., Stoer J., 1964, *Numerische Mathematik*, 6, 413
- Butterworth S., 1930, *Experimental Wireless & the Wireless Engineer*, 7, 536
- Chatterjee S., Ford E. B., Matsumura S., Rasio F. A., 2008, *ApJ*, 686, 580
- Chirikov B. V., 1979, *PhysRep*, 52, 263
- Das M., Green J. R., 2019, *Nature Communications*, 10, 2155
- Dejonghe H., Hut P., 1986, in Hut P., McMillan S. L. W., eds, *Lecture Notes in Physics*, Berlin Springer Verlag Vol. 267, *The Use of Supercomputers in Stellar Dynamics*. p. 212, doi:10.1007/BFb0116416
- Fousse L., Hanrot G., Lefèvre V., Pélissier P., Zimmermann P., 2007, *ACM Trans. Math. Softw.*, 33, 13–es
- Ghez A. M., et al., 2008, *ApJ*, 689, 1044
- Gillessen S., Eisenhauer F., Trippe S., Alexander T., Genzel R., Martins F., Ott T., 2009, *ApJ*, 692, 1075
- Goodman J., Heggie D. C., Hut P., 1993, *ApJ*, 415, 715
- Gravity Collaboration et al., 2019, *A&A*, 625, L10
- Hayes W. B., 2008, *MNRAS*, 386, 295
- Hénon M. H., 1971, *Ap&SS*, 14, 151
- Hoover W. G., Griswold Hoover C., 2017, arXiv e-prints, p. arXiv:1703.00470
- Hunter J. D., 2007, *Computing in Science & Engineering*, 9, 90
- Jones E., Oliphant T., Peterson P., et al., 2001–, SciPy: Open source scientific tools for Python, <http://www.scipy.org/>
- Jurić M., Tremaine S., 2008, *ApJ*, 686, 603
- Kandrup H. E., Vass I. M., Sideris I. V., 2003, *MNRAS*, 341, 927
- Killick R., Fearnhead P., Eckley I. A., 2012, *Journal of the American Statistical Association*, 107, 1590
- Laskar J., Gastineau M., 2009, *Nat*, 459, 817
- Mogavero F., Laskar J., 2022, *A&A*, 662, L3
- Oliphant T. E., 2006, *A guide to NumPy*. Vol. 1, Trelgol Publishing USA
- Pelupessy F. I., van Elteren A., de Vries N., McMillan S. L. W., Drost N., Portegies Zwart S. F., 2013, *A&A*, 557, A84
- Portegies Zwart S., 2020, *Nature Astronomy*, 4, 819
- Portegies Zwart S. F., Boekholt T. C. N., 2018, *Communications in Nonlinear Science and Numerical Simulations*, 61, 160
- Portegies Zwart S., McMillan S., 2018, *Astrophysical Recipes; The art of AMUSE*, doi:10.1088/978-0-7503-1320-9.
- Portegies Zwart S., McMillan S. L. W., van Elteren E., Pelupessy I., de Vries N., 2013, *Computer Physics Communications*, 183, 456
- Portegies Zwart S., et al., 2018, *AMUSE: the Astrophysical Multipurpose Software Environment*, doi:10.5281/zenodo.1443252, <https://doi.org/10.5281/zenodo.1443252>
- Portegies Zwart S. F., Boekholt T. C. N., Por E. H., Hamers A. S., McMillan S. L. W., 2022, *A&A*, 659, A86
- Rath J., Hadden S., Lithwick Y., 2022, *ApJ*, 932, 61
- Sridhar S., Touma J. R., 2016, *MNRAS*, 458, 4143
- Szebehely V., 1971, *Celestial Mechanics*, 4, 116
- Tamayo D., Murray N., Tremaine S., Winn J., 2021, *AJ*, 162, 220
- Van Rossum G., Drake F. L., 2009, *Python 3 Reference Manual*. CreateSpace, Scotts Valley, CA
- Wisdom J., 1980, *AJ*, 85, 1122

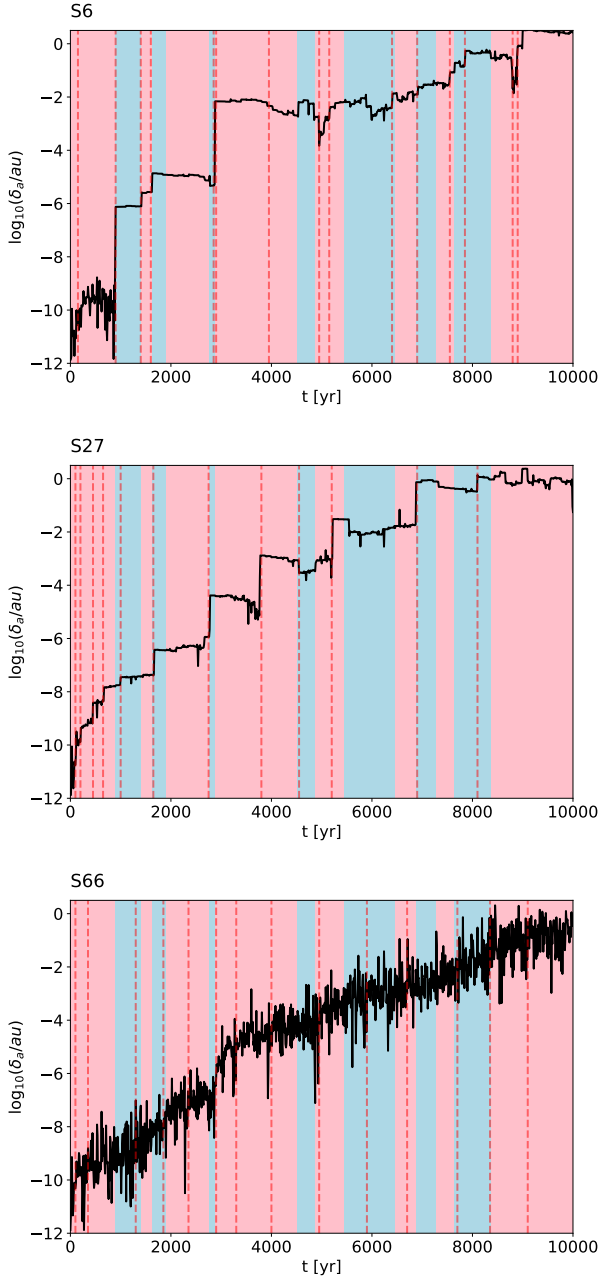


Figure 5. Evolution of the difference in semi-major axis between the two converged solutions, for individual stars. From top to bottom, we show the results for stars S6, S27 and S66, respectively. The vertical color bars are identical to those in figure 4. The vertical red dashed lines indicate the locations where the Pelt algorithm identifies the change in a as events for the individual stars. The big event at $t = 2876$ years is visible in S6 and S66, but for S27 the event is less pronounced. A slightly earlier event, at 2771 years (this event is not listed in table 1, but prominent in the right-hand panel in figure 8 for S21), is quite pronounced in S27, though. (It is to the left of the blue bar, whereas for S6 the event happens to the right side of the blue bar).

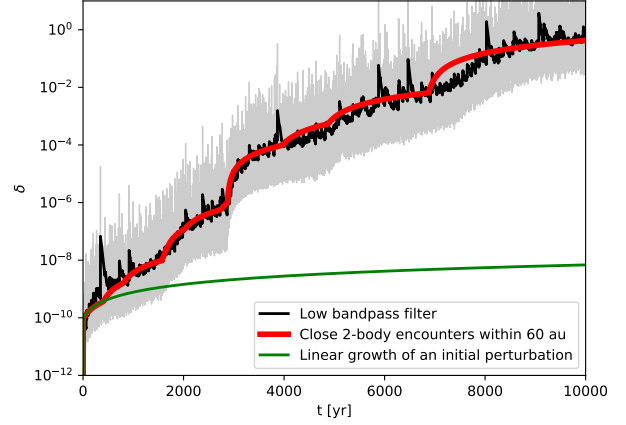


Figure 6. Normalized evolution of the phase-space distance (eq.6) for the S-stars as a function of time (gray) with in black the filtered version of the data (see also figure 3). Overplotted is the result of punctuated chaos with 13 close encounters (listed in Table 1) within $r_{ij} \approx 60$ au between two of the S-stars i and j at a distance $D \lesssim 1000$ au from the black hole (red). The green curve shows the result of ignoring all events, when the separation of the two orbits is driven by the initial displacement of star S5 by 15 m in the positive x -direction (cf.eq.2).

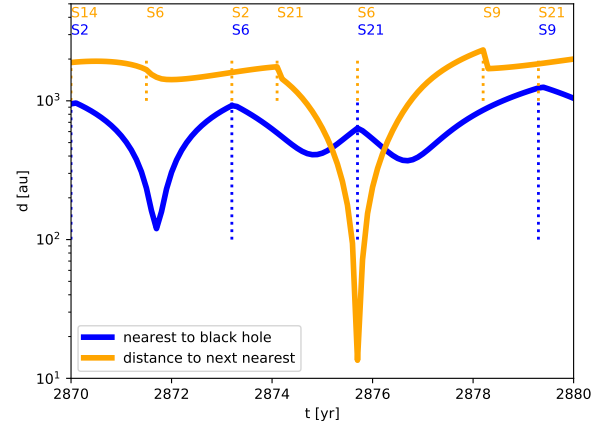


Figure 7. Closest distance between stars as a function of time from $t = 2870$ yr to $t = 2880$ yr. The blue curve gives the distance from the black hole to the nearest star (identified in blue at the top). The orange curve gives the separation between this nearest neighbor and the next-nearest star (identified at the top row on orange). The vertical dotted lines indicate when the nearest neighbor changes (blue) or the next nearest neighbor (orange). The closest distance between S6 and S21 is reached at ~ 2876 yr at a mutual distance of ~ 13.5 au within 635 au of the supermassive black hole.

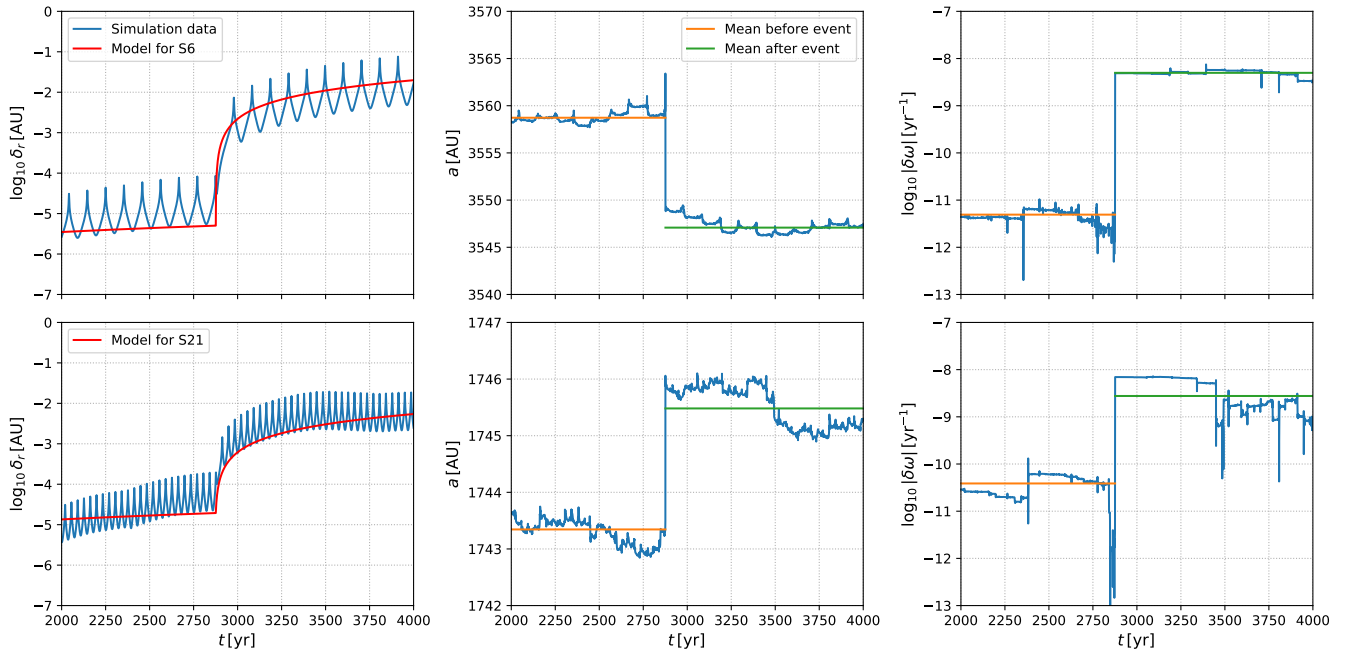


Figure 8. Illustration of an event driving the growth in separation between two solutions. We focus on the largest event at 2876 years, which was triggered by a close encounter between stars S6 (top row) and S21 (bottom row). From the simulation data, we plot the separation in position space (left column), semi-major axis of one of the two solutions (middle), and the absolute value of the difference in orbital frequency between them (right). We estimate mean values of a and $\delta\omega$ both before and after the event, which are sharply divided by the big event. Using these mean values, and the punctuated model for divergence from Sec. 2.2, we derive the analytical models for the evolution of δ_r (left column). Furthermore, the energy exchange between S6 and S21 is conservative (to within a percent). Notice that the bottom right figure for S21 shows both events: at 2771 years and 2876 years.

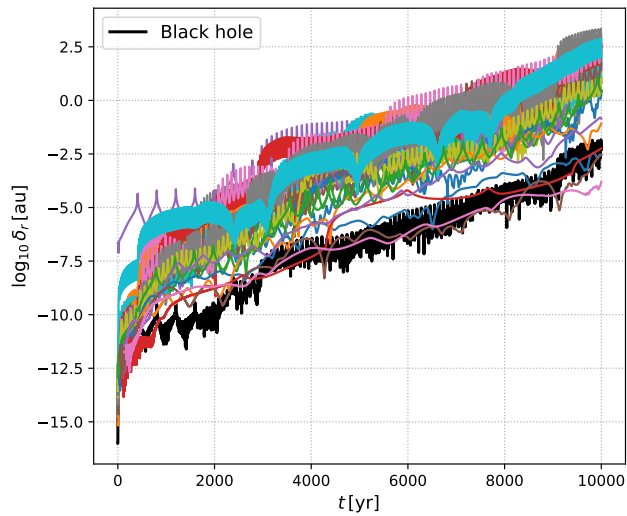


Figure 9. The time evolution of the separation in position space (δ_r) for each individual body, including the central black hole. On average, each body diverges at the same exponential rate. Note, however, that these curves were calculated by comparing the data from the two runs with $\epsilon = 10^{-21}$ and $\epsilon = 10^{-24}$ (rather than the perturbed and unperturbed solutions for $\epsilon = 10^{-24}$).